

# Optimal Operator preconditioning for hypersingular operator over 3D screens

R. Hiptmair and C. Jerez-Hanckes and C. Urzúa-Torres

Research Report No. 2016-09  
February 2016

Seminar für Angewandte Mathematik  
Eidgenössische Technische Hochschule  
CH-8092 Zürich  
Switzerland

# OPTIMAL OPERATOR PRECONDITIONING FOR HYPERANGULAR OPERATOR OVER 3D SCREENS

RALF HIPTMAIR, CARLOS JEREZ-HANCKES, CAROLINA URZÚA-TORRES

**Abstract.** We propose a new Calderón-type preconditioner for the hypersingular integral operator for  $-\Delta$  on screens in  $\mathbb{R}^3$ . We introduce a modified weakly singular operator, which is the exact inverse of the hypersingular operator on the unit disk. It forms the foundation for dual-mesh-based operator preconditioning. Applied to low-order boundary element Galerkin discretizations, it achieves  $h$ -uniformly bounded condition numbers. Heuristic extensions to general screens even with non-smooth boundaries are discussed. Their good performance is confirmed by numerical tests.

**1. Introduction.** We consider the exterior Laplace problem with Neumann boundary condition  $\mu$  on an open surface  $\Gamma \subset \mathbb{R}^3$ ,  $\Gamma$  having a boundary  $\partial\Gamma$  of positive measure: find  $U$  such that

$$-\Delta U = 0 \quad \text{in } \Omega := \mathbb{R}^3 \setminus \bar{\Gamma} \quad , \quad \frac{\partial U}{\partial n} = \mu \quad \text{on } \Gamma \quad , \quad (1.1)$$

plus appropriate decay conditions at infinity (*cf.* [17, Thm. 8.9]). This is the simplest case to consider for potential distributions on bounded objects which are infinitely thin in  $\mathbb{R}^3$ . Such problems are known in literature as hard screen problems and together with their soft (Dirichlet) counterparts, have been thoroughly investigated from a theoretical perspective.

A common numerical approach to model and numerically solve problems in unbounded homogeneous domains is the Boundary Element Method (BEM). Linchpin of its implementation are two ingredients: availability of a fundamental solution and Green's third identity which yields the so-called *integral representation*. In the homogeneous case, the latter allows to reconstruct  $U$  over the entire domain using exclusively boundary data via *single and double layer potentials*. When imposing boundary conditions, one derives Boundary Integral Equations (BIEs). The analysis of the arising Boundary Integral Operators (BIOs) in the framework of Sobolev spaces for screens is available for several problems, as elastic waves [25], acoustic scattering [24, 19], and electromagnetism [4]. Generally, one faces first-kind BIEs, which lead to ill-conditioned linear systems when discretized by low-order Galerkin BEM on fine meshes. Their solution via iterative solvers becomes prohibitively slow and thus demands preconditioning, for which several ideas have been proposed.

One approach to preconditioning is dubbed *opposite order* preconditioning. The idea comes from canceling the symbol order of the underlying pseudo-differential operator with optimal results when dealing with closed curves [23]. In the case of open arcs, since the weakly singular and hypersingular operators no longer map between the same pair of dual spaces, as for closed boundaries, the preconditioning performs sub-optimally. Specifically, a logarithmic growth with respect to the minimum mesh-width  $h_{min}$  is expected [18]. This is due to inverse inequalities [11, Thm. 2.2 and 3.6] between the norms of the related trace spaces –namely,  $H^{\pm\frac{1}{2}}$  and  $\tilde{H}^{\pm\frac{1}{2}}$ – required to bound the resulting condition number when applying operator preconditioning (*cf.* [10, Thm. 2.1]).

Further improvement was achieved by Bruno and Lintner [1] who introduced weights in the kernels of the BIOs. Such weights depend on the distance to  $\partial\Gamma$  and, by incorporating information on the singular behavior of the solution, overall performance is improved, as in augmented schemes [26]. Still, the extension of these ideas to smooth screens in 3D [2] has yet no rigorous numerical analysis.

Parallel to the above, exact variational inverses established in [15] for the line segment result in explicit Calderón-type preconditioners for open arcs [12]. These inverses are introduced as modified weakly singular and hypersingular operators, and one observes that they also incorporate the distance from  $\partial\Gamma$  in their kernels. Still, a major tool is the use of spectral decompositions using Chebyshev polynomials. Indeed, it allows to show that the difference between the kernel of the modified BIOs and the standard ones also reflects the gap between the norms of the standard trace spaces and tilde ones. Inspired by this approach and its applicability as preconditioners, one of the authors carried out preliminary research with J.-C. Nédélec on finding inverse relations analogous to the ones shown in [15]<sup>1</sup>.

In this paper, we propose a new Calderón preconditioner using dual mesh operator preconditioning [10], which yields optimal condition numbers for the BEM discretized hypersingular BIE on smooth screens in  $\mathbb{R}^3$ . This approach is shown to yield similar results for screens with corners, as for instance for squares, and for non-uniform meshes. Key is the solution of the hypersingular BIE provided by Fabrikant over the disk [6]. This is further discussed from the BIEs' setting by Li and Rong [16]. We interpret their findings as a modified weakly singular operator which is indeed the inverse of the hypersingular operator over the disk. As expected, this modification incorporates the distance to the boundary, in an analogous way to the function  $M(x, y)$  in the 2D case [15, eq. (3.3)]. For the sake of completeness, we will introduce some definitions and constraints regarding the discrete preconditioning and its extension to non-uniform meshes. However, some of the details are out of the scope of this article and we refer the reader to [14] for a detailed exposition.

It must be acknowledged that there is an entirely different approach to build preconditioners for screen problems arising from *subspace correction methods* [27, 9, 7]. Nonetheless, their analysis and comparison with Calderón preconditioning are left out for the sake of brevity.

The manuscript is structured as follows. In Section 2, we introduce definitions and notation. Section 2.1 recalls the BIE and properties of the underlying operators in the continuous case. BEM discretization and main theoretical results for non-uniform meshes are presented in Section 3. Moreover, two ideas are described to handle more general surfaces. Numerical results in Section 4 for canonical and several surfaces validate our claims. Conclusions and future work are given in Section 5.

**2. Preliminaries.** Let  $d = 1, 2, 3$ . For a bounded domain  $K \subseteq \mathbb{R}^d$ ,  $C^m(K)$ ,  $m \in \mathbb{N}$ , denotes the space of  $m$ -times differentiable scalar functions on  $K$ , and, similarly, for the space of infinitely differentiable, scalar continuous functions we write  $C^\infty(K)$ . In addition, Hölder spaces are referred to as  $C^{m,\alpha}(K)$ . Let  $L^p(K)$  denote the class of  $p$ -integrable functions over  $K$ . Dual spaces are defined in standard fashion with duality products denoted by angular brackets  $\langle \cdot, \cdot \rangle_K$ .

Let  $\mathcal{O} \in \mathbb{R}^d$ ,  $d = 2, 3$  be open and  $s \in \mathbb{R}$ . We denote standard Sobolev spaces by  $H^s(\mathcal{O})$ . For positive  $s$  and  $\mathcal{O}$  Lipschitz, let  $\tilde{H}^s(\mathcal{O})$  be the space of functions whose extension by zero over a closed domain  $\tilde{\mathcal{O}}$  belongs to  $H^s(\tilde{\mathcal{O}})$ , as in [15]. In particular, the following duality relations hold

$$\tilde{H}^{-1/2}(\mathcal{O}) \equiv \left( H^{1/2}(\mathcal{O}) \right)' \quad \text{and} \quad H^{-1/2}(\mathcal{O}) \equiv \left( \tilde{H}^{1/2}(\mathcal{O}) \right)'. \quad (2.1)$$

---

<sup>1</sup>Although to the best of our knowledge, the related research presented in the FEnICS conference in Paris 2014 is still work in progress, we must acknowledge it served as starting point for the results we present here.

**2.1. Variational Boundary Integral Equations on the Disk.** Throughout this section we focus on the circular disk  $\mathbb{D}_a$  with radius  $a > 0$ , defined as  $\mathbb{D}_a := \{\mathbf{x} \in \mathbb{R}^3 : x_3 = 0 \text{ and } \|\mathbf{x}\| < a\}$ . Thus, the volume problem domain becomes  $\Omega_a := \mathbb{R}^3 \setminus \bar{\mathbb{D}}_a$ . Often, we will use the following polar coordinate notation:  $\mathbf{x} = (r_x \cos \theta_x, r_x \sin \theta_x, 0) \in \mathbb{D}_a$ .

**2.1.1. Hypersingular Integral Equation.** We consider the following singular integral equation: for  $\mu \in C^1(\bar{\mathbb{D}}_a)$ , we seek a function  $u$  defined on  $\mathbb{D}_a$  such that

$$(\mathbb{W}u)(\mathbf{y}) := \frac{1}{4\pi} \int_{\mathbb{D}_a} u(\mathbf{x}) \frac{\partial^2}{\partial n_x \partial n_y} \frac{1}{\|\mathbf{x} - \mathbf{y}\|} d\mathbb{D}_a(\mathbf{x}) = \mu(\mathbf{y}), \quad \mathbf{y} \in \mathbb{D}_a, \quad (2.2)$$

where the dashed integral indicates that the expression above is to be interpreted as a Hadamard finite-part integral, with distributional meaning as in [17]. The measure  $d\mathbb{D}_a(\mathbf{x})$  denotes the surface element in terms of  $\mathbf{x} = (r_x \cos \theta_x, r_x \sin \theta_x, 0) \in \mathbb{D}_a$ , equal to  $ar_x dr_x d\theta_x$ , and the unknown  $u \in \tilde{H}^{1/2}(\mathbb{D}_a)$  is the jump of the Dirichlet trace of the solution  $U$  of the exterior Neumann problem (1.1) when  $\Omega = \Omega_a$ .

Let  $v(\mathbf{x})$ ,  $\mathbf{x} \in \mathbb{D}_a$ , be a continuously differentiable function, and let  $\tilde{v}$  be an appropriate extension of  $v$  into a three-dimensional neighborhood of  $\mathbb{D}_a$ . In order to write (2.2) in variational formulation, let us introduce the vectorial surfacic curl operator [22, p.133] as

$$\text{curl}_{\mathbb{D}_a} v(\mathbf{x}) := \mathbf{n}(\mathbf{x}) \times \nabla \tilde{v}(\mathbf{x}), \quad (2.3)$$

with  $\mathbf{n}(\mathbf{x})$  being the outer normal of  $\Gamma$  on  $\mathbf{x} \in \Gamma$ , and  $\nabla$  denoting the standard gradient.

**PROPOSITION 2.1.** *A symmetric variational formulation for (2.2) is given by: seek  $u \in \tilde{H}^{1/2}(\mathbb{D}_a)$  such that for all  $v \in \tilde{H}^{1/2}(\mathbb{D}_a)$*

$$\langle \mathbb{W}u, v \rangle_{\mathbb{D}_a} := \frac{1}{4\pi} \int_{\mathbb{D}_a} \int_{\mathbb{D}_a} \frac{\text{curl}_{\mathbb{D}_a} u(\mathbf{y}) \cdot \text{curl}_{\mathbb{D}_a} v(\mathbf{x})}{\|\mathbf{x} - \mathbf{y}\|} d\mathbb{D}_a(\mathbf{x}) d\mathbb{D}_a(\mathbf{y}) = \langle \mu, v \rangle_{\mathbb{D}_a}. \quad (2.4)$$

*Proof.* The proof follows the same steps as [22, Thm. 6.17] for closed surfaces. Since  $u, v \in \tilde{H}^{1/2}(\mathbb{D}_a)$ , when integrating by parts, the boundary term vanishes and [22, Lemma 6.16] still holds.  $\square$

**REMARK 1.** *Existence and uniqueness of solution of this problem was proved by Stephan in [24, Thm. 2.7]. Moreover, the bilinear form in (2.4) is  $\tilde{H}^{1/2}(\Gamma)$ -continuous and elliptic (cf. [19, Thm. 3.5.9]). One can show that in this case and for sufficiently smooth screens  $\Gamma$ , when approaching the edges  $\partial\Gamma$ , the solutions decay according to the square-root of the distance [5].*

**2.1.2. Modified Weakly Singular Integral Operator.** We define the modified weakly singular operator as

$$(\bar{\mathbb{V}}v)(\mathbf{x}) := -\frac{1}{4\pi} \int_{\mathbb{D}_a} v(\mathbf{y}) \frac{S(\mathbf{x}, \mathbf{y})}{\|\mathbf{x} - \mathbf{y}\|} d\mathbb{D}_a(\mathbf{y}), \quad \mathbf{x} \in \mathbb{D}_a, \quad (2.5)$$

where

$$S(\mathbf{x}, \mathbf{y}) := \frac{8}{\pi} \tan^{-1} \left( \frac{\sqrt{a^2 - r_x^2} \sqrt{a^2 - r_y^2}}{a \|\mathbf{x} - \mathbf{y}\|} \right), \quad \mathbf{x} \neq \mathbf{y}. \quad (2.6)$$

The reader must recall that the standard weakly singular BIO is given by (2.5) without the  $S(\mathbf{x}, \mathbf{y})$  term. In fact, since  $\lim_{\mathbf{x} \rightarrow \mathbf{y}} S(\mathbf{x}, \mathbf{y}) = 4$  when  $\mathbf{x}, \mathbf{y} \in \mathbb{D}_{a-\epsilon}$ ,  $\epsilon > 0$ , the kernels of  $\bar{\mathbf{V}}$  and  $\mathbf{V}$  have the same weakly singular behavior in (the interior of)  $\mathbb{D}_a$ . Also note that  $S(x, y) = 0$  if  $|\mathbf{x}| = a$  or  $|\mathbf{y}| = a$ . As a consequence,  $S$ , though bounded, will be discontinuous on  $\partial\mathbb{D}_a \times \partial\mathbb{D}_a$ .

The next fundamental result reveals why we are interested in this exotic looking integral operator.

PROPOSITION 2.2.  $\bar{\mathbf{V}} : H^{-1/2}(\mathbb{D}_a) \rightarrow \tilde{H}^{1/2}(\mathbb{D}_a)$  provides an exact inverse of  $\mathbf{W}$ .

Key tools for the proof of Proposition 2.2 are some auxiliary results by Li and Rong [16]. First, define the function  $p(k, \theta)$  as

$$p(k, \theta) := \frac{1}{2\pi} \sum_{n=-\infty}^{\infty} k^{|n|} e^{in\theta} = \frac{1}{2\pi} \frac{1 - k^2}{1 + k^2 - 2k \cos \theta}, \quad \forall |k| < 1, \quad (2.7)$$

with  $\theta \in [0, 2\pi]$  (cf. [6, Chap. 1.1]). This function allows us to rewrite the kernel of  $\bar{\mathbf{V}}$  as will be shown in the following Lemma.

LEMMA 2.1 (Lemma 1 [16]). *Let us consider points  $\mathbf{x}, \mathbf{y}$  on the disk  $\mathbb{D}_a$ , satisfying  $\mathbf{x} \neq \mathbf{y}$ , whose polar coordinates are given by  $\mathbf{x} = (r_x \cos \theta_x, r_x \sin \theta_x, 0) \in \mathbb{D}_a$  and equivalently for  $\mathbf{y}$ . Then for a parameter  $\alpha \in (0, 4)$ , such that  $\alpha \neq 2$ , it holds*

$$\frac{1}{4\pi} \frac{1}{\|\mathbf{x} - \mathbf{y}\|^\alpha} = \frac{1}{\pi} \sin \frac{\alpha\pi}{2} \int_0^{\min(r_x, r_y)} \frac{s^{\alpha-1}}{(r_x^2 - s^2)^{\alpha/2} (r_y^2 - s^2)^{\alpha/2}} p\left(\frac{s^2}{r_x r_y}, \theta_x - \theta_y\right) ds \quad (2.8)$$

$$= \frac{1}{\pi} \sin \frac{\alpha\pi}{2} \int_{\max(r_x, r_y)}^\infty \frac{s^{\alpha-1}}{(s^2 - r_x^2)^{\alpha/2} (s^2 - r_y^2)^{\alpha/2}} p\left(\frac{r_x r_y}{s^2}, \theta_x - \theta_y\right) ds. \quad (2.9)$$

Here the integrals above are understood in the sense of finite-part integrals if  $\alpha > 2$ .

We can now follow Fabrikant and introduce

$$L(k)u(r, \theta) := \int_0^{2\pi} p(k, \theta - \theta_0) u(r, \theta_0) d\theta_0 \quad (2.10)$$

$$= \frac{1}{2\pi} \sum_{n=-\infty}^{\infty} k^{|n|} e^{in\theta} \int_0^{2\pi} e^{-in\theta_0} u(r, \theta_0) d\theta_0, \quad (2.11)$$

with  $\theta \in [0, 2\pi]$ , and  $r \in [0, a]$ . This integral operator is sometimes called Poisson integral over the disk [6, Chap. 1.1]. The properties of  $L(k)u(r, \theta)$  combined with the formulae from Lemma 2.1 lead to a complete separation of variables. This fact plays a key role as the resulting expression for (2.2) will be an iterative system of Abel integral equations, whose solution is given in the next Theorem.

THEOREM 2.3 (Thm.2 [16]). *Let  $\mu \in C^1(\mathbb{D}_a)$ . Then, the solution  $u(\mathbf{x})$  of (2.2) can be expressed in terms of a two-dimensional improper integral as follows*

$$u(\mathbf{x}) = -\frac{1}{\pi} \int_{\mathbb{D}_a} \frac{\mu(\mathbf{y})}{R_{\mathbb{D}}(\mathbf{x}, \mathbf{y})} d\mathbb{D}_a(\mathbf{y}), \quad (2.12)$$

where

$$\frac{1}{R_{\mathbb{D}}(\mathbf{x}, \mathbf{y})} := 4 \int_{\max(r_x, r_y)}^a \frac{1}{(s^2 - r_x^2)^{1/2} (s^2 - r_y^2)^{1/2}} p\left(\frac{r_x r_y}{s^2}, \theta_x - \theta_y\right) ds. \quad (2.13)$$

REMARK 2. From (2.9) we notice that  $R_{\mathbb{D}}(\mathbf{x}, \mathbf{y})$  is a scaled restriction of  $\|\mathbf{x} - \mathbf{y}\|$  from  $\mathbb{R}^3$  to  $\mathbb{D}_a$ . Moreover, for  $a = \infty$ , Theorem 2.3 implies  $\frac{1}{R_{\mathbb{D}}(\mathbf{x}, \mathbf{y})} = \frac{1}{\|\mathbf{x} - \mathbf{y}\|}$ .

LEMMA 2.2 (Eq 1.2.14 in [6]). Let  $a > 0$ . If

$$a \geq t \geq \max(r_x, r_y), \quad r_x, r_y \in [0, a], \quad \text{and } \theta_x, \theta_y \in [0, 2\pi],$$

we find the following primitive

$$\begin{aligned} \int \frac{1}{(t^2 - r_x^2)^{1/2}(t^2 - r_y^2)^{1/2}} p\left(\frac{r_x r_y}{t^2}, \theta_x - \theta_y\right) dt \\ = \frac{1}{2\pi} \frac{1}{\|\mathbf{x} - \mathbf{y}\|} \tan^{-1} \left( \frac{\sqrt{t^2 - r_x^2} \sqrt{t^2 - r_y^2}}{t \|\mathbf{x} - \mathbf{y}\|} \right). \end{aligned}$$

*Proof.* This can be shown by direct calculation.  $\square$

Combining the above elements we can prove the next result.

PROPOSITION 2.4. When  $\mu$  in (2.2) is continuously differentiable, the solution of the hypersingular integral equation can be written as  $u(\mathbf{x}) = (\bar{\nabla}\mu)(\mathbf{x})$ , for all  $\mathbf{x} \in \mathbb{D}_a$ .

*Proof.* Using Theorem 2.3, we get that the solution to (2.2) can be written as (2.12). Moreover, when  $a < \infty$ , we may use Lemma 2.2, to write

$$\begin{aligned} -\frac{1}{\pi} \frac{1}{R_{\mathbb{D}}(\mathbf{x}, \mathbf{y})} &= -\frac{4}{\pi} \int_{\max(r_x, r_y)}^a \frac{1}{(s^2 - r_x^2)^{1/2}(s^2 - r_y^2)^{1/2}} p\left(\frac{r_x r_y}{s^2}, \theta_x - \theta_y\right) ds \\ &= -\frac{2}{\pi^2} \frac{1}{\|\mathbf{x} - \mathbf{y}\|} \tan^{-1} \left( \frac{\sqrt{s^2 - r_x^2} \sqrt{s^2 - r_y^2}}{s \|\mathbf{x} - \mathbf{y}\|} \right) \Big|_{\max(r_x, r_y)}^a \\ &= -\frac{2}{\pi^2} \frac{1}{\|\mathbf{x} - \mathbf{y}\|} \left\{ \tan^{-1} \left( \frac{\sqrt{a^2 - r_x^2} \sqrt{a^2 - r_y^2}}{a \|\mathbf{x} - \mathbf{y}\|} \right) - \tan^{-1}(0) \right\} \\ &= -\frac{1}{4\pi} \frac{1}{\|\mathbf{x} - \mathbf{y}\|} \frac{8}{\pi} \tan^{-1} \left( \frac{\sqrt{a^2 - r_x^2} \sqrt{a^2 - r_y^2}}{a \|\mathbf{x} - \mathbf{y}\|} \right) = -\frac{1}{4\pi} \frac{S(\mathbf{x}, \mathbf{y})}{\|\mathbf{x} - \mathbf{y}\|}, \end{aligned}$$

as stated.  $\square$

Finally, we need to extend the above result to the corresponding fractional Sobolev space. We do this via the following Corollary and subsequent Proposition.

COROLLARY 2.5.  $W\bar{\nabla} = \text{Id}$  in  $H^{-1/2}(\mathbb{D}_a)$ .

*Proof.* Follows from the previous Proposition combined with density of  $C^\infty(\bar{\mathbb{D}}_a)$  in  $H^{-1/2}(\mathbb{D}_a)$ .  $\square$

PROPOSITION 2.6.  $\bar{\nabla} : H^{-1/2}(\mathbb{D}_a) \rightarrow \tilde{H}^{1/2}(\mathbb{D}_a)$  is continuous.

*Proof.* Let us assume that  $\bar{\nabla} : H^{-1/2}(\mathbb{D}_a) \rightarrow \tilde{H}^{1/2}(\mathbb{D}_a)$  is not a bounded operator. Then, by virtue of density, there exists a sequence  $(\mu_n)_n \in C^\infty(\bar{\mathbb{D}}_a)$  such that

$$\|\mu_n\|_{H^{-1/2}(\mathbb{D}_a)} = 1, \quad \|\bar{\nabla}\mu_n\|_{\tilde{H}^{1/2}(\mathbb{D}_a)} \rightarrow \infty, \quad \text{as } n \rightarrow \infty. \quad (2.14)$$

Since  $W : \tilde{H}^{1/2}(\mathbb{D}_a) \rightarrow H^{-1/2}(\mathbb{D}_a)$  is an isomorphism (cf. Remark 1), it holds

$$\|\bar{V}\mu_n\|_{\tilde{H}^{1/2}(\mathbb{D}_a)} \leq C \|W\bar{V}\mu_n\|_{H^{-1/2}(\mathbb{D}_a)} \stackrel{(Corollary 2.5)}{=} C \|\mu_n\|_{H^{-1/2}(\mathbb{D}_a)}, \quad (2.15)$$

from where we get a contradiction.  $\square$

Now we are finally in the position to use the above results and density arguments to conclude the assertion of Proposition 2.2.

**COROLLARY 2.7.** *The bilinear form  $\langle \bar{V}\vartheta, \mu \rangle_{\mathbb{D}_a}$ ,  $\vartheta, \mu \in H^{-1/2}(\mathbb{D}_a)$  is  $H^{-1/2}(\mathbb{D}_a)$ -elliptic and continuous.*

*Proof.* Follows from continuity and ellipticity of  $W$  combined with Proposition 2.2.  $\square$

### 3. Preconditioning Strategy.

**3.1. Operator Preconditioning.** Let us consider the continuous bilinear form  $\mathbf{a} \in \mathcal{L}(\tilde{H}^{1/2}(\Gamma) \times \tilde{H}^{1/2}(\Gamma), \mathbb{R})$  induced by  $W$ . Following the policy of operator preconditioning [10], we can build our preconditioning strategy by finding a continuous bilinear form  $\mathbf{b} \in \mathcal{L}(H^{-1/2}(\Gamma) \times H^{-1/2}(\Gamma), \mathbb{R})$ , and finite dimensional spaces  $X_h \subset \tilde{H}^{1/2}(\Gamma)$  and  $Y_h \subset H^{-1/2}(\Gamma)$  such that:

- (P1)  $\mathbf{a}$ ,  $\mathbf{b}$  and the  $L^2$ -duality pairing  $\mathbf{t}$  satisfy discrete inf-sup conditions with constants  $c_A, c_B, c_T > 0$  respectively, on the corresponding discrete spaces; and,
- (P2)  $\dim X_h = M = \dim Y_h$ .

Choosing any bases of  $X_h$  and  $Y_h$ , then the associated Galerkin matrices  $\mathbf{A}_h, \mathbf{B}_h$ , and  $\mathbf{T}_h$  satisfy [10, Thm. 2.1]

$$\kappa(\mathbf{T}_h^{-1} \mathbf{B}_h \mathbf{T}_h^{-T} \mathbf{A}_h) \leq \frac{\|\mathbf{a}\| \|\mathbf{b}\| \|\mathbf{t}\|^2}{c_A c_B c_T^2}, \quad (3.1)$$

where  $\kappa$  designates the spectral condition number.

**3.2. Discretization.** We can choose boundary element spaces  $X_h$  and  $Y_h$  to satisfy the condition  $M = \dim X_h = \dim Y_h$  by using a dual mesh based on the approach of Buffa-Christiansen [3] and Steinbach [21, Chap 2.1]. In particular, we first mesh our screen  $\Gamma$  and denote the resulting primal mesh by  $\Gamma_h$ . We then build a barycentric refinement  $\bar{\Gamma}_h$  as illustrated in Figure 3.1, and finally construct the dual mesh  $\hat{\Gamma}_h$  by combining the barycentric elements, as shown in Figure 3.2. Since the dual mesh preconditioning technique is well established, we skip details and refer to [3, 14].

We build the corresponding discrete spaces by choosing low order Lagrangian boundary element functions, i.e.

- $X_h :=$  space of continuous piecewise linear functions on  $\Gamma_h$ ,  
satisfying zero boundary conditions on  $\partial\Gamma$ .
- $\bar{X}_h :=$  space of continuous piecewise linear functions on  $\bar{\Gamma}_h$ ,  
satisfying zero boundary conditions on  $\partial\Gamma$ .
- $Y_h :=$  space of piecewise constants functions on  $\hat{\Gamma}_h$ .
- $\bar{Y}_h :=$  space of piecewise constants functions on  $\bar{\Gamma}_h$ .

Thus  $M = \dim X_h = \dim Y_h$  equals the number of interior nodes in  $\Gamma_h$ .

Instead of building our Galerkin matrices directly over  $\hat{\Gamma}_h$ , we compute the barycentric refinement  $\bar{\Gamma}_h$  and introduce the *averaging matrix*  $\mathbf{C}_d : \bar{Y}_h \rightarrow Y_h$  to

**Fig. 3.1:** Barycentric refinement for triangles and quadrilaterals. On the left we illustrate the 6 obtained children elements for a triangular element, while on the right we show the 4 children elements in the case of quadrilaterals. Original primal nodes are in red dots, center of mass is depicted in green diamond and blue x's are used for mid-edge nodes.

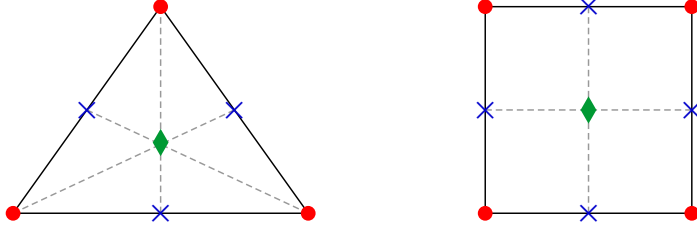
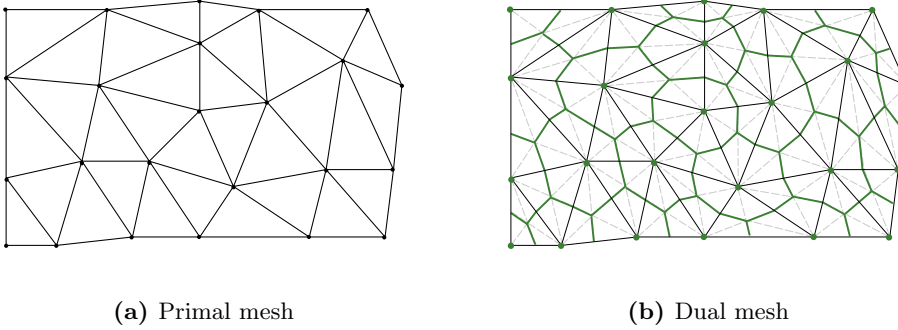


**Fig. 3.2:** Primal and dual meshes. Black lines show primal elements, dashed gray lines barycentric ones, and green lines are used to highlight dual cells.



construct the basis functions of  $Y_h$  as a linear combination of barycentric basis functions of  $\bar{Y}_h$ .

Then we build the Galerkin matrix of the modified weakly singular  $\bar{V}$  over the dual mesh  $\hat{\Gamma}_h$  as follows: Let  $\bar{\mathbf{V}}_b : \bar{Y}_h \rightarrow \bar{Y}_h$  be the Galerkin matrix of  $\bar{V}$  computed over the barycentric refinement  $\bar{\Gamma}_h$ , then we can write  $\bar{\mathbf{V}}_h = \mathbf{C}_d^T \bar{\mathbf{V}}_b \mathbf{C}_d$ .

Analogously, we introduce the *coupling matrix*  $\mathbf{C}_p : \bar{X}_h \rightarrow X_h$  to connect barycentric basis functions corresponding to  $\bar{X}_h$  to those of the *primal* basis functions  $X_h$ .<sup>2</sup>

The construction and representation of these linking matrices are discussed in [14]. However, in order to illustrate their use, let  $\mathbf{M}_b : \bar{X}_h \rightarrow \bar{Y}_h$  be the mass matrix computed over the barycentric mesh. By using the above matrices, it is clear that the Galerkin matrix  $\mathbf{T}_h$  associated to the  $L^2$ -duality pairing  $\mathfrak{t}$  is given by  $\mathbf{T}_h = \mathbf{C}_p^T \mathbf{M}_b^T \mathbf{C}_d^T$ .

**3.3. Stability of Discrete Duality Pairing on Non-Uniform Triangular Meshes.** As mentioned in Remark 1, the solutions of screen problems have a singular behavior near the boundary, which can be resolved by refining the mesh towards it.

<sup>2</sup>We borrow their name from [20]. However, we change the notation for the sake of clarity:  $\mathbf{C}_p$  ( $\mathbf{C}_d$ ) stands for primal (dual), to honor the space to which the matrix connects the associated barycentric boundary element space.



Consequently, we are interested in applying the operator preconditioning strategy to non-uniform meshes. For this purpose, we adapt the work developed by O. Steinbach in [21] and introduce some of the notation therein.

The key tool is the preservation of the inf-sup condition related to the dual pairing  $\mathbf{t}$ , in this case the  $L^2$ -inner product over  $\Gamma$ . This entails maintaining the  $H^1$ -stability of a generalized  $L^2$ -projection  $\tilde{Q}_h$ , defined via a Petrov-Galerkin approach [21, 14].

**ASSUMPTION 3.1.** *We consider a shape regular and locally quasi-uniform family of primal meshes  $\{\Gamma_h\}_{h \in \mathbb{H}}$ ,  $h > 0$  of  $\Gamma$ , whose members are labelled by  $h$  from an index set  $\mathbb{H}$ .*

Let us consider a given primal mesh  $\Gamma_h$ , and denote the mesh-width of an arbitrary element  $\tau_l \in \Gamma_h$  by  $h_l$ . We equip  $X_h$  with the standard locally supported nodal basis functions. As a consequence of local quasi-uniformity, we can introduce for each basis function  $\varphi_k \in X_h$ , an associated mesh size  $\hat{h}_k$  satisfying

$$\frac{1}{c_Q} \leq \frac{\hat{h}_k}{h_l} \leq c_Q \quad \text{for all } l \text{ such that } \tau_l \cap \text{supp}\{\varphi_k\} \neq \emptyset, k = 1, \dots, M, \quad (3.2)$$

with a global constant  $c_Q \geq 1$ . Now, for an arbitrary  $\tau_l \in \Gamma_h$ , define the set

$$J(l) := \{k \in \{1, \dots, M\} : \text{supp}\{\varphi_k\} \cap \tau_l \neq \emptyset\}. \quad (3.3)$$

**ASSUMPTION 3.2.** *We assume our primal mesh  $\Gamma_h$  satisfies the following local mesh condition:*

$$\frac{51}{7} - \sqrt{\sum_{k_1 \in J(l)} \hat{h}_{k_1} \sum_{k_2 \in J(l)} \hat{h}_{k_2}^{-1}} \geq c_0 > 0 \quad \forall \tau_l \in \Gamma_h, \quad (3.4)$$

with a global positive constant  $c_0$  [21, eq. (2.30)].

**THEOREM 3.3.** *Let Assumptions 3.1 and 3.2 be satisfied. Then, the discrete inf-sup condition:*

$$\sup_{v_h \in Y_h} \frac{|\langle w_h, v_h \rangle_\Gamma|}{\|v_h\|_{H^{-1/2}(\Gamma)}} \geq \frac{1}{c_s} \|w_h\|_{\tilde{H}^{1/2}(\Gamma)}, \quad \forall w_h \in X_h, h \in \mathbb{H}, h > 0. \quad (3.5)$$

holds with a positive constant  $c_s$  independent of  $h$ .

*Proof.* Follows the same steps as in [21, Theorem 2.1 and 2.2]. The required extensions are analogous to those developed in [12] and are detailed in [14].  $\square$

**REMARK 3.** *Assumption 3.1 can be shown to imply the local non-degeneracy condition [3, Prop.3.11] required for the inf-sup condition when using the dual mesh construction by Buffa and Christiansen. The proof is given in [14].*

**3.4. Operator Preconditioning over the Unit Disk.** We can now apply the operator preconditioning strategy described in Section 3.1 over the unit disk to obtain:

**COROLLARY 3.4.** *Let Assumptions 3.1 and 3.2 hold. Let  $\mathbf{W}_h$  be the Galerkin matrix arising from the bilinear form (2.2) over  $\Gamma_h$ . Let  $\bar{\mathbf{V}}_h$  be the Galerkin matrix of  $\bar{\mathbf{V}}$  over the dual mesh  $\hat{\Gamma}_h$ , and  $\mathbf{T}_h$  the  $L^2$ -dual pairing constructed as above. Then, when preconditioning  $\mathbf{W}_h$  by the matrix product  $\bar{\mathbf{P}}_h = \mathbf{T}_h^{-1} \bar{\mathbf{V}}_h \mathbf{T}_h^{-T}$ , we get*

$$\kappa(\bar{\mathbf{P}}_h \mathbf{W}_h) \leq C, \quad (3.6)$$

with  $C$  a constant independent of  $h$ .

We now extend the above idea to more general screens  $\Gamma \subset \mathbb{R}^3$  such that there are at least bi-Lipschitz mappings  $\phi : \mathbb{D}_1 \rightarrow \bar{\Gamma}$ . As a consequence,  $\Gamma$  will be an orientable  $C^{0,1}$ -manifold with boundary  $\partial\Gamma$ . Observe that in a variational setting it holds  $\phi^* = \phi^{-1}$ .

REMARK 4. *The bi-Lipschitz mapping  $\phi : \mathbb{D}_1 \rightarrow \bar{\Gamma}$  allow us to use the fact that the spaces  $\tilde{H}^{1/2}(\Gamma)$ ,  $H^{1/2}(\Gamma)$ ,  $H^{-1/2}(\Gamma)$ , and  $\tilde{H}^{-1/2}(\Gamma)$  are invariant under the pullback  $\phi^* : L^2(\mathbb{D}_1) \rightarrow L^2(\Gamma)$ .*

**3.5. Unit Disk Based Preconditioner for Mapped Screens.** We can generalize the setting of operator preconditioning over the unit disk by lifting the variational problem to an open surface  $\Gamma$  defined by a  $C^1$ -diffeomorphism  $\phi : \mathbb{D}_1 \rightarrow \bar{\Gamma}$ . For instance, consider the hypersingular integral operator.

For the sake of clarity, we introduce additional notation for this section. Let us denote the hypersingular integral operator on the unit disk by  $W_{\mathbb{D}_1}$ , and that on  $\Gamma = \phi(\mathbb{D}_1)$  by  $W_\Gamma$ , i.e.

$$(W_\Gamma u)(\mathbf{x}) := \int_\Gamma k_W(\mathbf{x}, \mathbf{y}) u(\mathbf{y}) d\Gamma(\mathbf{y}), \quad \mathbf{x} \in \Gamma, u \in \tilde{H}^{1/2}(\Gamma), \quad (3.7)$$

where  $k_W(\mathbf{x}, \mathbf{y}) := \frac{1}{4\pi} \frac{\partial^2}{\partial n_x \partial n_y} \frac{1}{\|\mathbf{x} - \mathbf{y}\|}$  is the kernel of  $W$ . It can be pulled back to  $\mathbb{D}_1$  using the parametrization:

$$(W_\Gamma^* \hat{u})(\phi(\hat{\mathbf{x}})) := \int_{\mathbb{D}_1} k_W(\phi(\hat{\mathbf{x}}), \phi(\hat{\mathbf{y}})) \hat{u}(\hat{\mathbf{y}}) \sqrt{\det(D\phi(\hat{\mathbf{y}})^T D\phi(\hat{\mathbf{y}}))} d\mathbb{D}_1(\hat{\mathbf{y}}), \quad \hat{\mathbf{x}} \in \mathbb{D}_1, \quad (3.8)$$

where  $D\phi(\hat{\mathbf{x}})$  denotes the Jacobian of  $\phi$  on  $\hat{\mathbf{x}}$ , and  $\hat{u} \in \tilde{H}^{1/2}(\mathbb{D}_1)$  is the pull-back of  $u$  to  $\mathbb{D}_1$ . Here we assume finite local distortion:

$$\|\phi(\hat{\mathbf{x}}) - \phi(\hat{\mathbf{y}})\| \approx \|\hat{\mathbf{x}} - \hat{\mathbf{y}}\|, \quad (3.9a)$$

$$\exists c_\phi, C_\phi > 0 : c_\phi \leq \det(D\phi^T D\phi) \leq C_\phi, \quad \text{a.e.}, \quad (3.9b)$$

$$\phi \in W^{1,\infty}(\mathbb{D}_1), \text{ and } \phi^{-1} \in W^{1,\infty}(\Gamma). \quad (3.9c)$$

Let now  $\bar{V}_{\mathbb{D}_1}$  denote the modified weakly singular operator over the disk. Then it holds

$$\bar{V}_{\mathbb{D}_1} W_\Gamma^* = \text{Id} + \bar{V}_{\mathbb{D}_1} (W_\Gamma^* - W_{\mathbb{D}_1}) : \tilde{H}^{1/2}(\mathbb{D}_1) \rightarrow \tilde{H}^{1/2}(\mathbb{D}_1), \quad (3.10)$$

which is continuous. On the other hand, one can deduce

$$\langle W_\Gamma^* \hat{u}, \hat{u} \rangle_{\mathbb{D}_1} = \langle W_\Gamma \phi^{-*}(\hat{u}), \phi^{-*}(\hat{u}) \rangle_\Gamma \geq c \|\phi^{-*}(\hat{u})\|_{\tilde{H}^{1/2}(\Gamma)}^2, \quad (3.11)$$

for all  $\hat{u} \in \tilde{H}^{1/2}(\mathbb{D}_1)$ . In addition, by (3.9c), it holds

$$\|\phi^{-*}(\hat{u})\|_{L^2(\Gamma)} = \|u\|_{L^2(\Gamma)} \approx \|\hat{u}\|_{L^2(\mathbb{D}_1)}, \quad (3.12a)$$

$$|\phi^{-*}(\hat{u})|_{H^1(\Gamma)} = |u|_{H^1(\Gamma)} \approx |\hat{u}|_{H^1(\mathbb{D}_1)}, \quad (3.12b)$$

and therefore, by interpolation arguments, we get the same for  $\tilde{H}^{1/2}(\Gamma)$  and thus, the operator is elliptic. From these two properties one can conclude the following statement.

COROLLARY 3.5.  $\bar{V}_{\mathbb{D}_1}$  still induces a suitable bilinear form to build a preconditioner for  $W_*$  adopting the procedures of our preconditioning strategy.

However, it is important to point out that the condition number bound (3.1) will be affected by a constant depending on  $\phi$  and the distortion effected by it. We will see later on in numerical experiments that this causes a pre-asymptotic phase in which the behavior of the preconditioner is not as good as expected. For this reason, in the next two subsections, we discuss some heuristic modifications to improve the preconditioner.

**3.6. Shape-aware Preconditioner for Flat Screens.** Let us consider again the disk  $\mathbb{D}_a$  of radius  $a$  centered at the origin. The kernel  $k_{\bar{V}}$  of  $\bar{V}$  over  $\mathbb{D}_a$  is given by

$$k_{\bar{V}}(\mathbf{x}, \mathbf{y}) := -\frac{S(\mathbf{x}, \mathbf{y})}{\|\mathbf{x} - \mathbf{y}\|}, \quad \text{with } S(\mathbf{x}, \mathbf{y}) = \frac{8}{\pi} \tan^{-1} \left( \frac{\sqrt{a^2 - r_x^2} \sqrt{a^2 - r_y^2}}{a \|\mathbf{x} - \mathbf{y}\|} \right) \quad (3.13)$$

for  $\mathbf{x} \neq \mathbf{y}$ , and using the polar coordinates notation introduced in section 2.1.

Note that the boundary of the disk  $\mathbb{D}_a$  is given in polar coordinates as  $r = a(\theta)$ . Then, the kernel of the modified weakly singular integral operator can be rewritten with

$$S(\mathbf{x}, \mathbf{y}) = \frac{8}{\pi} \tan^{-1} \left( \frac{\sqrt{a(\theta_x)^2 - r_x^2} \sqrt{a(\theta_y)^2 - r_y^2}}{\sqrt{a(\theta_x) a(\theta_y)} \|\mathbf{x} - \mathbf{y}\|} \right), \quad \mathbf{x} \neq \mathbf{y}. \quad (3.14)$$

Although  $a(\theta) = a$  for  $\mathbb{D}_a$  –and the expression above is unduly complicated–, it can be used as a starting point to develop an approximation of  $W^{-1}$  for general surfaces that allow polar angle parametrization of their boundary. We point out that the flat screen need not be the result of a transformed unit disk via a  $C^1$ -diffeomorphism as in the previous subsection. However, a piecewise Lipschitz transformation is still required.

REMARK 5. *This can be regarded as an interpretation of Fabrikant's approximation for more general flat screens discussed in [6, Section 3.3].*

**3.7. Shape-aware Preconditioner for Parametrized Screens.** Recall from (3.13) the kernel  $k_{\bar{V}}$  of  $\bar{V}$  over the disk  $\mathbb{D}_a$ , use  $r_x = \|\mathbf{x}\|$ , and rewrite  $S(\mathbf{x}, \mathbf{y})$  as

$$S(\mathbf{x}, \mathbf{y}) = \frac{8}{\pi} \tan^{-1} \left( \frac{\sqrt{a^2 - \|\mathbf{x}\|^2} \sqrt{a^2 - \|\mathbf{y}\|^2}}{a \|\mathbf{x} - \mathbf{y}\|} \right), \quad \mathbf{x} \neq \mathbf{y}, \quad (3.15)$$

Since

$$\phi : \begin{cases} \mathbb{D}_1 \rightarrow \mathbb{D}_a \\ \hat{\mathbf{x}} \mapsto a\hat{\mathbf{x}} \end{cases}, \quad \phi^{-1} : \begin{cases} \mathbb{D}_a \rightarrow \mathbb{D}_1 \\ \mathbf{x} \mapsto \mathbf{x}/a \end{cases},$$

$S(\mathbf{x}, \mathbf{y})$  can be rephrased over  $\mathbb{D}_1$  as

$$S_{\phi}(\hat{\mathbf{x}}, \hat{\mathbf{y}}) := \frac{8}{\pi} \tan^{-1} \left( \frac{\sqrt{\|\phi(\frac{\hat{\mathbf{x}}}{\|\hat{\mathbf{x}}\|})\|^2 - \|\phi(\hat{\mathbf{x}})\|^2} \sqrt{\|\phi(\frac{\hat{\mathbf{y}}}{\|\hat{\mathbf{y}}\|})\|^2 - \|\phi(\hat{\mathbf{y}})\|^2}}{\sqrt{g_{\phi}(\hat{\mathbf{x}}) g_{\phi}(\hat{\mathbf{y}})} \|\phi(\hat{\mathbf{x}}) - \phi(\hat{\mathbf{y}})\|} \right), \quad (3.16)$$

for  $\hat{\mathbf{x}} \neq \hat{\mathbf{y}}$ , and where  $g_{\phi}(\hat{\mathbf{x}})$  is the Gram determinant of  $\phi$  on  $\hat{\mathbf{x}}$ . This expression is somehow analogous to the approach developed in Section 3.6 with  $a(\theta_x) = \phi(\frac{\hat{\mathbf{x}}}{\|\hat{\mathbf{x}}\|})$ .

**Table 4.1:** Results for  $\mathbf{W}_h$  over the unit disk screen: quasi-uniform meshes.

(a) Triangular mesh				(b) Quadrilateral mesh			
N	$\kappa(\mathbf{W}_h)$	$\kappa(\mathbf{P}_h \mathbf{W}_h)$	$\kappa(\overline{\mathbf{P}}_h \mathbf{W}_h)$	N	$\kappa(\mathbf{W}_h)$	$\kappa(\mathbf{P}_h \mathbf{W}_h)$	$\kappa(\overline{\mathbf{P}}_h \mathbf{W}_h)$
16	2.02	1.22	1.22	32	2.12	1.70	1.35
64	3.32	1.87	1.41	128	3.95	2.07	1.41
256	6.64	2.25	1.44	512	8.56	2.47	1.47
1024	13.68	2.66	1.45	2048	18.2	2.89	1.49

On the other hand, we could map from  $\mathbb{D}_a$  to  $\mathbb{D}_1$  instead, since  $S(\mathbf{x}, \mathbf{y})$  can be rewritten as

$$S(\mathbf{x}, \mathbf{y}) = \frac{8}{\pi} \tan^{-1} \left( \frac{\sqrt{1 - \left\| \frac{\mathbf{x}}{a} \right\|^2} \sqrt{1 - \left\| \frac{\mathbf{y}}{a} \right\|^2} \frac{a}{\|\mathbf{x} - \mathbf{y}\|}}{\right)}, \quad \mathbf{x} \neq \mathbf{y}, \quad (3.17)$$

and recast as

$$S_{\phi^*}(\mathbf{x}, \mathbf{y}) := \frac{8}{\pi} \tan^{-1} \left( \frac{\sqrt{1 - \|\phi^*(\mathbf{x})\|^2} \sqrt{1 - \|\phi^*(\mathbf{y})\|^2} \sqrt{g_{\phi}(\mathbf{x})g_{\phi}(\mathbf{y})}}{\|\mathbf{x} - \mathbf{y}\|} \right), \quad (3.18)$$

for  $\mathbf{x} \neq \mathbf{y}$ . Then, we will base our preconditioner on an approximate modified weakly singular operator  $\overline{\mathbf{V}}$ , for which  $S(\mathbf{x}, \mathbf{y})$  is replaced by  $S_{\phi^*}(\mathbf{x}, \mathbf{y})$  in the kernel of (2.5). This approach has the advantage of enforcing axisymmetry and being directly implementable on the given mesh  $\Gamma_h$ .

**4. Numerical Experiments.** We compare the performance of our preconditioner  $\overline{\mathbf{P}}_h := \mathbf{T}_h^{-1} \overline{\mathbf{V}}_h \mathbf{T}_h^{-T}$  with opposite order operator preconditioning arising from using the standard weakly singular operator  $\mathbf{V}$ , i.e.  $\mathbf{P}_h := \mathbf{T}_h^{-1} \mathbf{V}_h \mathbf{T}_h^{-T}$ . The numerical experiments were implemented using BETL2[13]. The measured condition numbers were computed via the ratio of the maximum and minimum eigenvalues, i.e. for a matrix  $\mathbf{A}_h$ , we have  $\kappa(\mathbf{A}_h) := \lambda_{max}/\lambda_{min}$ .

**4.1. Unit Disk.** Table 4.1 shows condition numbers obtained by both preconditioners over a unit disk using homogeneous quasi-uniform triangular and quadrilateral meshes. Neglecting the expected numerical error due to numerical quadrature, the modified weakly singular operator as a preconditioner performs independently of  $h$ , matching the predicted asymptotic optimality behavior. The clustering of the eigenvalues of the considered boundary element Galerkin matrices is illustrated in Figures 4.1a-4.1b.

Next we consider non-uniform meshes. Table 4.2 shows the condition numbers obtained by both preconditioners over a unit disk using two different locally refined triangular meshes (see Figure 4.2). Once again our preconditioner seems to achieve  $h$ -independent condition numbers. Figures 4.3a-4.3b illustrate the clustering of eigenvalues.

**4.2. Unit Disk Based Preconditioner for Mapped Screens.** We conduct numerical experiments for two mapped screens which will be identified by the applied transformation  $\phi$ , described via cartesian coordinates  $\hat{\mathbf{x}} = (x_0, x_1) \in \mathbb{D}_1$ . Figure 4.4 displays obtained spectra as well as Table 4.3 presents resulting condition numbers

**Fig. 4.1:** Eigenvalue distributions. The spectrum of the matrix  $\mathbf{W}_h$  is shown in black, while that obtained by preconditioning with  $\mathbf{V}_h$  is in red. Blue depicts the resulting spectrum when preconditioning by  $\bar{\mathbf{V}}_h$ .

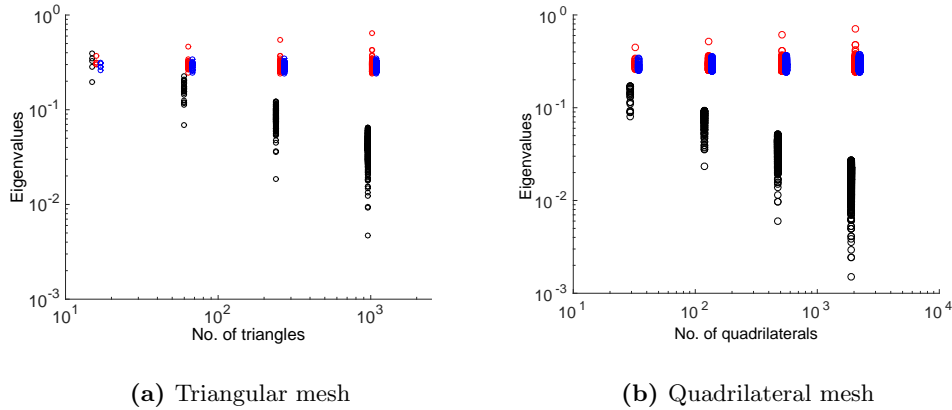


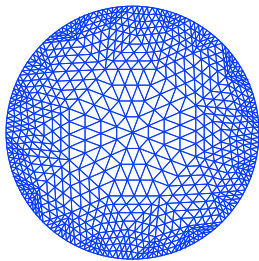
**Table 4.2:** Results for  $\mathbf{W}_h$  over the unit disk screen: non-uniform meshes

(a) Mesh A				(b) Mesh B			
N	$\kappa(\mathbf{W}_h)$	$\kappa(\mathbf{P}_h \mathbf{W}_h)$	$\kappa(\bar{\mathbf{P}}_h \mathbf{W}_h)$	N	$\kappa(\mathbf{W}_h)$	$\kappa(\mathbf{P}_h \mathbf{W}_h)$	$\kappa(\bar{\mathbf{P}}_h \mathbf{W}_h)$
92	2.56	1.93	1.27	498	15.33	3.07	1.67
384	6.66	2.47	1.38	1992	28.60	3.34	1.55
1536	12.26	2.92	1.38				

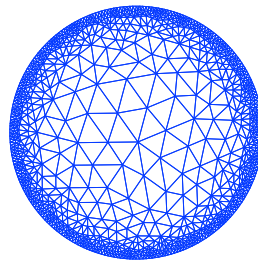
**Fig. 4.2:** Locally refined triangular meshes

(a) Mesh A was created using the functions `Attraction` and `Threshold` iteratively in `Gmsh` [8]. This means the mesh size is a *piecewise linear* function of the distance to the disk’s boundary.

(b) Mesh B was constructed with the functions `Attraction` and `Matheval` in `Gmsh` [8], where the evaluated function was the *continuous* distance to the boundary of the disk.



$\bar{\mathbf{x}}$



$\bar{\mathbf{x}}$

**Fig. 4.3:** Spectrum of standard  $\mathbf{W}_h$  is shown in black, while the preconditioned by  $\mathbf{V}_h$  is in red, and the one corresponding to  $\bar{\mathbf{V}}_h$  is in blue.

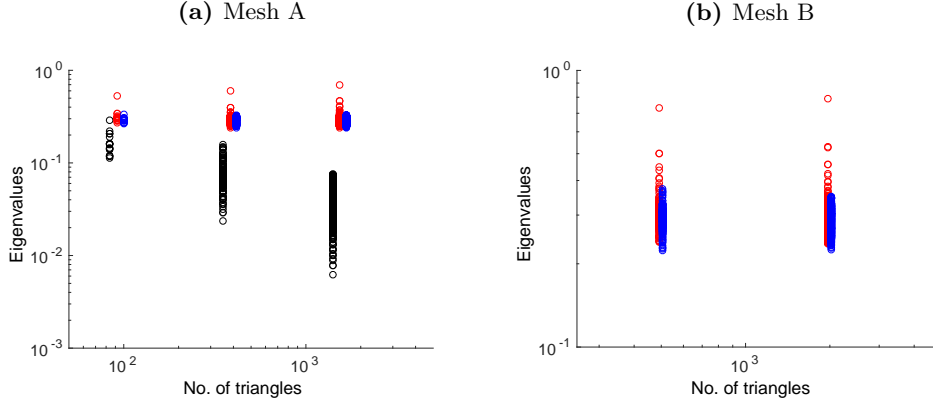


**Table 4.3:** Results for  $\mathbf{W}_h$  over mapped screens.

(a)  $\phi(\hat{\mathbf{x}}) = (x_0, x_1, x_0 + x_1)^T$

(b)  $\phi(\hat{\mathbf{x}}) = (x_0, x_1, x_0^2 + x_1^2)^T$

N	$\kappa(\mathbf{W}_h)$	$\kappa(\mathbf{P}_h \mathbf{W}_h)$	$\kappa(\bar{\mathbf{P}}_h \mathbf{W}_h)$
52	2.05	1.64	1.65
208	3.91	2.07	1.89
832	8.04	2.46	1.98
3328	16.79	2.87	2.03

N	$\kappa(\mathbf{W}_h)$	$\kappa(\mathbf{P}_h \mathbf{W}_h)$	$\kappa(\bar{\mathbf{P}}_h \mathbf{W}_h)$
16	3.02	1.22	2.02
64	6.17	1.67	2.63
256	14.35	1.97	2.99
1024	32.94	2.35	3.22

when applying  $\mathbf{P}_h = \mathbf{T}_h^{-1} \mathbf{V}_h \mathbf{T}_h^{-T}$  and  $\bar{\mathbf{P}}_h = \mathbf{T}_h^{-1} \bar{\mathbf{V}}_h \mathbf{T}_h^{-T}$ , the latter implemented as discussed in Section 3.5. Therefore, we follow (3.10), and build our Galerkin matrix  $\bar{\mathbf{V}}_h$  on the unit disk  $\mathbb{D}_1$ . In both cases, our proposal seems to be in a pre-asymptotic phase due to the effect of the geometry on the condition number bound (3.1). It follows that the asymptotic optimality can fail to have a practical meaning.

**4.3. Shape-aware Preconditioner for Flat Screens.** We report the results for a unit square using the approach proposed in Section 3.6. Here we considered the following radius function:

$$a(\theta) := \begin{cases} 1/\cos \theta, & -\pi/4 < \theta < \pi/4 \\ 1/\sin \theta, & \pi/4 < \theta < 3\pi/4 \\ -1/\cos \theta, & 3\pi/4 < \theta < 5\pi/4 \\ -1/\sin \theta, & 5\pi/4 < \theta < 7\pi/4 \end{cases}, \quad (4.1)$$

to be used in (3.14) to build our preconditioner  $\bar{\mathbf{P}}_h$ .

Table 4.4 contains the resulting condition numbers for both triangular and quadrilateral meshes. Furthermore, we also include the corresponding results for a locally refined triangular mesh, shown in Table 4.5 and its corresponding figure. Although the results are slightly worse than on the unit disk, one can observe that the construction of the preconditioning operator as discussed in (3.14) yields a satisfactory preconditioner.

**Fig. 4.4:** Eigenvalue distribution. The spectrum of matrix  $\mathbf{W}_h$  is shown in black, while that preconditioned by  $\mathbf{V}_h$  is depicted in red. The one corresponding to  $\bar{\mathbf{V}}_h$  is in blue.

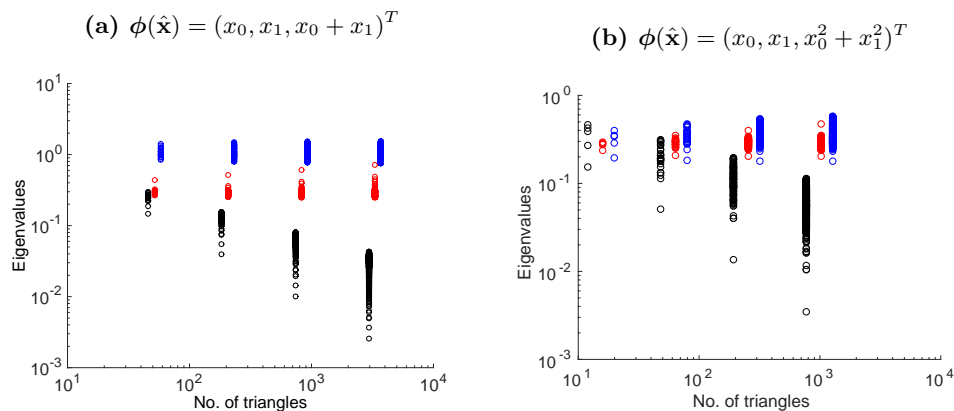


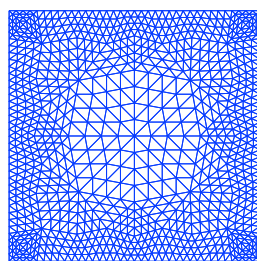
**Table 4.4:** Results for  $\mathbf{W}_h$  over a square screen using shape-aware preconditioner for flat screens: quasi-uniform meshes.

(a) Triangular mesh				(b) Quadrilateral mesh			
N	$\kappa(\mathbf{W}_h)$	$\kappa(\mathbf{P}_h \mathbf{W}_h)$	$\kappa(\bar{\mathbf{P}}_h \mathbf{W}_h)$	N	$\kappa(\mathbf{W}_h)$	$\kappa(\mathbf{P}_h \mathbf{W}_h)$	$\kappa(\bar{\mathbf{P}}_h \mathbf{W}_h)$
16	1.36	1.26	1.22	16	1.52	1.45	1.27
64	2.53	2.02	1.39	64	2.49	1.91	1.41
256	4.87	2.44	1.44	256	4.93	2.32	1.48
1024	9.79	2.87	1.48	1024	9.85	2.74	1.51

**Table 4.5:** Results for  $\mathbf{W}_h$  over the unit square screen using shape-aware preconditioner for flat screens: locally refined mesh.

N	$\kappa(\mathbf{W}_h)$	$\kappa(\mathbf{P}_h \mathbf{W}_h)$	$\kappa(\bar{\mathbf{P}}_h \mathbf{W}_h)$
108	4.02	2.29	1.46
432	7.21	2.64	1.50
1728	14.54	3.08	1.56

**Fig. 4.5:** Locally refined mesh used for numerical experiments displayed in Table 4.5.



$\hat{\mathbf{x}}$

In addition, we present numerical experiments for different flat triangular screens: equilateral, right isosceles and a right triangle whose minimal angle is  $30^\circ$ . We can observe from Tables 4.6–4.8, that the shape-aware preconditioner for flat screens performs well. Furthermore, the pre-asymptotic phase seems to be extended when the minimal angle decreases, which is expected due to the geometry deformation with respect to the unit disk  $\mathbb{D}_1$  and the consequent increase on the constant related to

(3.1). The corresponding spectra are shown in Figures 4.6–4.8, using the same color convention as in Figure 4.4.

**Table 4.6:** Results for  $\mathbf{W}_h$  over equilateral triangle screen using shape-aware preconditioner for flat screen : quasi-uniform triangular mesh.

N	$\kappa(\mathbf{W}_h)$	$\kappa(\mathbf{P}_h \mathbf{W}_h)$	$\kappa(\overline{\mathbf{P}}_h \mathbf{W}_h)$
74	2.51	2.03	1.47
296	5.18	2.38	1.40
1184	11.11	2.87	1.40

**Fig. 4.6:** Spectrum for equilateral triangle.

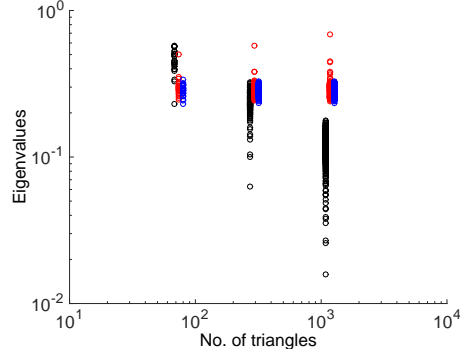


**Table 4.7:** Results for  $\mathbf{W}_h$  over right isosceles triangle screen using shape-aware preconditioner for flat screen : quasi-uniform triangular mesh.

N	$\kappa(\mathbf{W}_h)$	$\kappa(\mathbf{P}_h \mathbf{W}_h)$	$\kappa(\overline{\mathbf{P}}_h \mathbf{W}_h)$
60	2.25	1.80	1.25
240	4.68	2.31	1.33
960	9.68	2.79	1.36

**Fig. 4.7:** Spectrum for isosceles triangle.

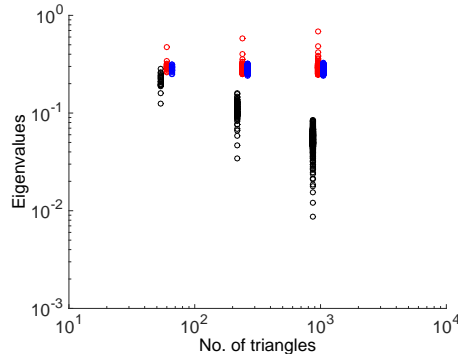
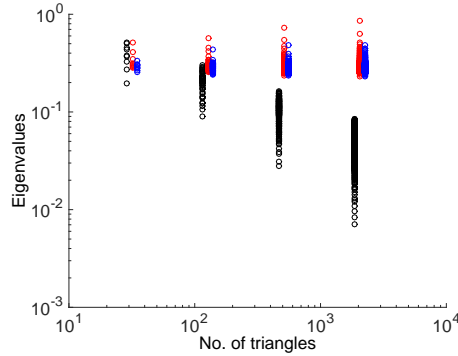


**Table 4.8:** Results for  $\mathbf{W}_h$  over right triangle screen using shape-aware preconditioner for flat screen : quasi-uniform triangular mesh

N	$\kappa(\mathbf{W}_h)$	$\kappa(\mathbf{P}_h \mathbf{W}_h)$	$\kappa(\overline{\mathbf{P}}_h \mathbf{W}_h)$
32	2.62	1.82	1.29
128	3.39	2.20	1.79
512	5.83	3.07	2.02
2048	12.05	3.70	2.10

**Fig. 4.8:** Spectrum for right triangle.



**4.4. Shape-aware Preconditioner for Parametrized Screens.** Tables 4.10–4.11 show the condition numbers obtained for  $\mathbf{W}_h$  alone, preconditioned by opposite order ( $\mathbf{P}_h$ ) and by our approach ( $\overline{\mathbf{P}}_h$ ). Recall from Section 3.7, that we build  $\overline{\mathbf{P}}_h$  by using the Galerkin matrix arising from the approximate  $\overline{\mathbf{V}}$  given by (3.16). We identify



each considered parametrized screen via its transformation  $\phi$ , which is described using cartesian coordinates  $\hat{\mathbf{x}} = (x_0, x_1) \in \mathbb{D}_1$ .

Let  $g_\phi^+$  and  $g_\phi^-$  denote the upper and lower bound of the Gram determinant  $g_\phi$ . Table 4.9 summarizes some information to be considered when analyzing the results for the different screens. We observe that for larger ratios  $g_\phi^+/g_\phi^-$ , the pre-asymptotic phase has a bigger effect on the preconditioner's performance, which is consistent with what we expect from (3.10).

**Table 4.9:** Summary of considered parametrized screens and the corresponding bounds for their Gram determinants.

Table id.	$\phi(\hat{\mathbf{x}})$	$(g_\phi^-)^2$	$(g_\phi^+)^2$
4.10a	$(x_0, x_1, x_0 + x_1)^T$	3	3
4.10b	$(x_0, 2x_1, x_0 + 2x_1)^T$	12	12
4.10c	$(x_0, x_1, x_0^2 + x_1^2)^T$	1	5
4.10d	$(x_0, 2x_1, \frac{x_0^2 + x_1^2}{2})^T$	1	2
4.11a	$(x_0, x_1, x_0 x_1)^T$	1	2
4.11b	$(x_0, x_1, \exp(\frac{x_0 + x_1}{2}))^T$	1.5	3.06
4.11c	$(x_0, 2x_1, \exp(x_0 + 2x_1))^T$	8	282
4.11d	$(x_0, 2x_1, \exp(\frac{x_0 + 2x_1}{2}))^T$	3	17.68

**Table 4.10:** Results for  $\mathbf{W}_h$  over parametrized screens.  $\bar{\mathbf{P}}_h$  built using shape-aware preconditioner for parametrized screens.

(a)  $\phi(\hat{\mathbf{x}}) = (x_0, x_1, x_0 + x_1)^T$

N	$\kappa(\mathbf{W}_h)$	$\kappa(\mathbf{P}_h \mathbf{W}_h)$	$\kappa(\bar{\mathbf{P}}_h \mathbf{W}_h)$
52	2.05	1.64	1.18
208	3.91	2.07	1.27
832	8.04	2.46	1.29
3328	16.79	2.87	1.30

(b)  $\phi(\hat{\mathbf{x}}) = (x_0, 2x_1, x_0 + 2x_1)^T$

N	$\kappa(\mathbf{W}_h)$	$\kappa(\mathbf{P}_h \mathbf{W}_h)$	$\kappa(\bar{\mathbf{P}}_h \mathbf{W}_h)$
26	1.69	1.54	1.26
104	3.14	1.98	1.39
416	6.62	2.42	1.48
1664	14.23	2.84	1.53

(c)  $\phi(\hat{\mathbf{x}}) = (x_0, x_1, x_0^2 + x_1^2)^T$

N	$\kappa(\mathbf{W}_h)$	$\kappa(\mathbf{P}_h \mathbf{W}_h)$	$\kappa(\bar{\mathbf{P}}_h \mathbf{W}_h)$
16	3.02	1.22	1.62
64	6.17	1.67	1.91
256	14.35	1.97	1.98
1024	32.94	2.35	2.01

(d)  $\phi(\hat{\mathbf{x}}) = (x_0, 2x_1, \frac{x_0^2 + x_1^2}{2})^T$

N	$\kappa(\mathbf{W}_h)$	$\kappa(\mathbf{P}_h \mathbf{W}_h)$	$\kappa(\bar{\mathbf{P}}_h \mathbf{W}_h)$
16	2.22	1.14	1.33
64	4.04	1.69	1.55
256	8.57	1.99	1.57
1024	18.92	2.33	1.58

**Table 4.11:** Results for  $\mathbf{W}_h$  over parametrized screens.  $\bar{\mathbf{P}}_h$  built using shape-aware preconditioner for parametrized screens.

(a) $\phi(\hat{\mathbf{x}}) = (x_0, x_1, x_0x_1)^T$				(b) $\phi(\hat{\mathbf{x}}) = (x_0, x_1, \exp(\frac{x_0+x_1}{2}))^T$			
N	$\kappa(\mathbf{W}_h)$	$\kappa(\mathbf{P}_h\mathbf{W}_h)$	$\kappa(\bar{\mathbf{P}}_h\mathbf{W}_h)$	N	$\kappa(\mathbf{W}_h)$	$\kappa(\mathbf{P}_h\mathbf{W}_h)$	$\kappa(\bar{\mathbf{P}}_h\mathbf{W}_h)$
16	2.11	1.27	1.18	16	2.02	1.24	1.18
64	3.72	1.88	1.41	64	2.44	1.84	1.40
256	8.10	2.25	1.44	256	7.40	2.19	1.44
1024	18.21	2.64	1.44	1024	15.78	2.56	1.44

(c) $\phi(\hat{\mathbf{x}}) = (x_0, 2x_1, \exp(x_0 + 2x_1))^T$				(d) $\phi(\hat{\mathbf{x}}) = (x_0, 2x_1, \exp(\frac{x_0+2x_1}{2}))^T$			
N	$\kappa(\mathbf{W}_h)$	$\kappa(\mathbf{P}_h\mathbf{W}_h)$	$\kappa(\bar{\mathbf{P}}_h\mathbf{W}_h)$	N	$\kappa(\mathbf{W}_h)$	$\kappa(\mathbf{P}_h\mathbf{W}_h)$	$\kappa(\bar{\mathbf{P}}_h\mathbf{W}_h)$
26	4.68	1.78	1.57	26	1.83	1.55	1.27
104	12.06	2.23	1.76	104	3.91	1.94	1.37
416	33.53	2.74	1.94	416	9.10	2.37	1.48
1664	79.75	3.23	2.11	1664	20.35	2.78	1.56

**5. Conclusion.** Based on integral operators with an explicit kernel that supply exact inverses for hypersingular operators on disks, we have developed operator preconditioning on screens in  $\mathbb{R}^3$ . Our numerical results confirm the asymptotic optimality of our preconditioner with respect to both uniform and locally refined meshes. The achievable condition numbers depend on the extent of deformation with respect to the unit disk  $\mathbb{D}_1$  and can increase considerably depending on the transformation  $\phi$ . In order to overcome the possibly degraded performance of our approach, we propose two alternatives for preconditioning on a general screen, which, in numerical tests, show superior performance, though a more rigorous analysis is still missing.

Current and future work involves implementing a preconditioner for  $\mathbb{V}$  based on its exact inverse on the disk given by a modified hypersingular operator  $\bar{\mathbb{W}}$ .

#### REFERENCES

- [1] O. P. BRUNO AND S. K. LINTNER, *Second-kind integral solvers for TE and TM problems of diffraction by open arcs*, Radio Science, 47 (2012), p. 6006.
- [2] O. P. BRUNO AND S. K. LINTNER, *A high-order integral solver for scalar problems of diffraction by screens and apertures in three-dimensional space*, J. Comput. Phys., 252 (2013), pp. 250–274.
- [3] A. BUFFA AND S. CHRISTIANSEN, *A dual finite element complex on the barycentric refinement*, Mathematics of Computation, 76 (2007), pp. 1743–1769.
- [4] A. BUFFA AND S. H. CHRISTIANSEN, *The electric field integral equation on Lipschitz screens: definitions and numerical approximation*, Numer. Math., 94 (2003), pp. 229–267.
- [5] M. COSTABEL, M. DAUGE, AND R. DUDUCHAVA, *Asymptotics without logarithmic terms for crack problems*, Comm. Partial Differential Equations, 28 (2003), pp. 869–926.
- [6] V. I. FABRIKANT, *Mixed boundary value problems of potential theory and their applications in engineering*, vol. 68 of Mathematics and its Applications, Kluwer Academic Publishers Group, Dordrecht, 1991.
- [7] M. FEISCHL, T. FÜHRER, N. HEUER, M. KARKULIK, AND D. PRAETORIUS, *Adaptive boundary element methods*, Archives of Computational Methods in Engineering, (2014), pp. 1–81.
- [8] C. GEUZAIN AND J.-F. REMACLE, *Gmsh: A 3-D finite element mesh generator with built-in pre- and post-processing facilities*, Internat. J. Numer. Methods Engrg., 79 (2009), pp. 1309–1331.

- [9] N. HEUER, *Preconditioners for the p-version of the boundary element Galerkin method in  $\mathbb{R}^3$* , habilitation, Uni Hannover, 1998.
- [10] R. HIPTMAIR, *Operator preconditioning*, Computers and Mathematics with Applications, 52 (2006), pp. 699–706.
- [11] R. HIPTMAIR, C. JEREZ-HANCKES, AND S. MAO, *Extension by zero in discrete trace spaces: inverse estimates*, Math. Comp., 84 (2015), pp. 2589–2615.
- [12] R. HIPTMAIR, C. JEREZ-HANCKES, AND C. URZÚA-TORRES, *Mesh-independent operator preconditioning for boundary elements on open curves.*, SIAM J. Numerical Analysis, 52 (2014), pp. 2295–2314.
- [13] R. HIPTMAIR AND L. KIELHORN, *BETL - A generic boundary element template library*, tech. rep., SAM - Seminar for Applied Mathematics, ETH Zurich., 2012.
- [14] R. HIPTMAIR AND C. URZÚA-TORRES, *Dual Mesh Operator Preconditioning Over 3D Screens: Low Order Lagrangian Discretization.*, Tech. Rep. 2016-XX, Seminar for Applied Mathematics, ETH Zürich, Switzerland, 2015.
- [15] C. JEREZ-HANCKES AND J. NÉDÉLEC, *Explicit variational forms for the inverses of integral logarithmic operators over an interval*, SIAM Journal on Mathematical Analysis, 44 (2012), pp. 2666–2694.
- [16] X.-F. LI AND E.-Q. RONG, *Solution of a class of two-dimensional integral equations*, J. Comput. Appl. Math., 145 (2002), pp. 335–343.
- [17] W. MCLEAN, *Strongly Elliptic Systems and Boundary Integral Equations*, Cambridge University Press, Cambridge, UK, 2000.
- [18] W. MCLEAN AND O. STEINBACH, *Boundary element preconditioners for a hypersingular integral equations on an interval*, Adv. Comp. Math., 11 (1999), pp. 271–286.
- [19] S. SAUTER AND C. SCHWAB, *Boundary Element Methods*, vol. 39 of Springer Series in Computational Mathematics, Springer, Heidelberg, 2010.
- [20] Y. SMIRNOVA, *Dual mesh Calderón preconditioning for single layer boundary integral operator*, tech. rep., SAM - Seminar for Applied Mathematics, ETH Zurich., 2012.
- [21] O. STEINBACH, *Stability estimates for hybrid coupled domain decomposition methods*, vol. 1809 of Lecture Notes in Mathematics, Springer-Verlag, Berlin, 2003.
- [22] ———, *Numerical approximation methods for elliptic boundary value problems: Finite and boundary elements*, Springer, New York, 2008. Finite and boundary elements, Translated from the 2003 German original.
- [23] O. STEINBACH AND W. WENDLAND, *The construction of some efficient preconditioners in the boundary element method*, Adv. Comput. Math, 9 (1998), pp. 191–216.
- [24] E. STEPHAN, *Boundary integral equations for screen problems in  $\mathbb{R}^3$* , Integral Equations and Operator Theory, 10 (1987), pp. 236–257.
- [25] E. P. STEPHAN, *A boundary integral equation method for three-dimensional crack problems in elasticity*, Math. Methods Appl. Sci., 8 (1986), pp. 609–623.
- [26] E. P. STEPHAN AND W. L. WENDLAND, *An augmented Galerkin procedure for the boundary integral method applied to two-dimensional screen and crack problems*, Applicable Anal., 18 (1984), pp. 183–219.
- [27] T. TRAN AND E. P. STEPHAN, *Additive schwarz methods for the h-version boundary element method*, Applicable Analysis, 60 (1996), pp. 63–84.